Phys Chem Minerals (1987) 14:13–20

PHYSICS AND CHEMISTRY OF MINERALS

High-Pressure Crystal Chemistry of Chrysoberyl, Al_2BeO_4: Insights on the Origin of Olivine Elastic Anisotropy

Robert M. Hazen
Carnegie Institution of Washington, Geophysical Laboratory, 2801 Upton St., NW, Washington, DC 20008, USA

Abstract. High-pressure crystal structure refinements and axial compressibilities have been determined by x-ray methods for the olivine isomorph chrysoberyl, Al_2BeO_4. Unlike silicate olivines, which are more than twice as compressible along *b* than along *a*, chrysoberyl (space group *Pbnm*) has nearly isotropic compressibility with $\beta_a = 1.12 \pm 0.04$, $\beta_b = 1.46 \pm 0.05$, and $\beta_c = 1.31 \pm 0.03$ (all $\times 10^{-4}$ kbar^{-1}). The resultant bulk modulus is 2.42 ± 0.05 Mbar, with K' assumed to be 4. The axial compression ratios of chrysoberyl are 1.00:1.30:1.17, compared to axial compression ratios 1.00:2.02:1.60 for forsterite. These differences in compression anisotropy arise from differences in relative bond compressibilities. In chrysoberyl the average aluminum-oxygen and beryllium-oxygen bond compressibilities are similar, yielding nearly isotropic compression, but in silicate olivines octahedral cation-oxygen bonds are significantly more compressible than Si–O bonds, so that compression parallel to *a* is much more restricted than that parallel to *b*. The inherent anisotropy of the olivine structure is not, by itself, sufficient to cause anisotropic compression. It appears that in the case of olivine the distribution of cations of different valences, in conjunction with the structure type, leads to anisotropies in physical properties.

Key words: Chrysoberyl, compressibility, high-pressure structure, equation-of-state, elasticity.

Introduction

Olivine is one of the most elastically anisotropic of all mantle silicates, with compressional velocities along the *a* crystallographic axis more than 30 percent greater than along *b* (Kumazawa and Anderson 1969; Graham and Barsch 1969; Sumino et al. 1977; Shimizu et al. 1982; Suzuki et al. 1983). These unusually large anisotropies may complicate interpretation of seismic data from olivine-rich regions, particularly if crystals adopt a preferred orientation. Conversely, identification of large seismic anisotropies within the earth may provide an indicator of the distribution of olivine, as well as of the mineral's predominant crystallographic orientation.

All silicate olivines ($R_2^{2+}SiO_4$: R = Mg, Fe, Mn, Ca, Ni) appear to display similar compressional anisotropies, with $C_{11} \gg C_{33} > C_{22}$. It might be concluded, therefore, that these differences are an inherent trait of the orthorhombic olivine-type structure; however, the olivine isomorph chrysoberyl (Al_2BeO_4) displays more nearly isotropic elastic moduli (Wang et al. 1975). The anisotropy observed for silicate olivines, therefore, is not solely dependent upon the topological arrangement of atoms.

High-pressure crystallography is a method sufficiently sensitive to document the structural changes that result in anisotropic compression. Previous studies of the olivines forsterite (Hazen and Finger 1980; Kudoh and Takeuchi 1985), fayalite (Hazen 1977; Kudoh and Takeda 1986), and monticellite (Sharp et al. 1986), for example, suggest that differences between compressibilities of silicon-oxygen bonds versus M1 octahedral magnesium- or iron-oxygen bonds lead to the observed macroscopic compressional anisotropies. The primary objective of the present study is to determine high-pressure crystal structures of chrysoberyl in order to compare the high-pressure structural behavior of this mineral with that of the silicate olivines.

Experimental

Specimen Description

Crystals of natural chrysoberyl from Colatina, Espirito Santo, Brazil (National Museum of Natural History, Smithsonian Institution #R15231) were selected from the same material employed by Barton (1986) in his thermochemical studies of minerals in the $BeO-Al_2O_3-SiO_2-H_2O$ system. This specimen contains 3.1 weight percent Fe_2O_3, which substitutes for Al_2O_3 and corresponds to about 2.5 mole percent Fe_2BeO_4. Crystal fragments of dimensions approximately $100 \times 100 \times 40$ μm were selected for x-ray diffraction study at room and high pressure.

Data Collection at Room Pressure

Chrysoberyl unit cell parameters at room pressure (Table 1) were refined from diffractometer angles of twenty reflections, each of which was centered in eight equivalent crystal

Table 1. Unit-cell parameters of chrysoberyl at several pressures

Pressure	a (Å)	b (Å)	c (Å)	V (Å^3)	V/Vo
0.001	4.428 (1)[a]	9.415 (3)	5.481 (2)	228.5 (1)	1.0000
14.0[b]	4.421 (1)	9.399 (3)	5.471 (1)	227.3 (1)	0.9949
31.5	4.413 (2)	9.373 (4)	5.458 (1)	225.8 (1)	0.9880
40.0	4.407 (1)	9.366 (3)	5.453 (1)	225.1 (1)	0.9851
54.0	4.400 (1)	9.343 (3)	5.442 (1)	223.7 (1)	0.9789
62.5	4.398 (1)	9.329 (3)	5.436 (1)	223.0 (1)	0.9760

[a] Parenthesized figures represent *esd*'s
[b] Pressure esd's are ±1 kbar

Table 2. Chrysoberyl refinement conditions and refined parameters

		1 bar	14 kbar	31.5 kbar	40 kbar	54 kbar	62.5 kbar
Number of Obs. ($I>2\sigma$)		223	135	133	118	124	207
R^b (%)		3.3	4.9	3.7	4.5	5.3	3.8
Weighted R^b (%)		2.4	3.3	2.7	2.6	3.6	3.3
Extinction,[c] r^* ($\times 10^5$)		15.5 (8)[a]	33 (3)	32 (3)	29 (2)	28 (3)	28 (2)
Atom	Parameter						
Al1	x	0	0	0	0	0	0
	y	0	0	0	0	0	0
	z	0	0	0	0	0	0
	B	0.55 (3)	0.97 (6)	0.78 (5)	0.86 (6)	0.75 (7)	0.86 (5)
Al2	x	0.9942 (4)	0.9939 (6)	0.9947 (7)	0.9953 (7)	0.9940 (8)	0.9937 (3)
	y	0.2729 (1)	0.2733 (3)	0.2732 (2)	0.2729 (3)	0.2720 (3)	0.2731 (2)
	z	0.25	0.25	0.25	0.25	0.25	0.25
	B	0.37 (3)	0.73 (7)	0.72 (5)	0.59 (6)	0.57 (7)	0.66 (5)
Be	x	0.4328 (13)	0.4295 (24)	0.4291 (18)	0.4309 (23)	0.4332 (26)	0.4333 (16)
	y	0.0930 (6)	0.0888 (16)	0.0935 (13)	0.0902 (18)	0.0895 (20)	0.0902 (12)
	z	0.25	0.25	0.25	0.25	0.25	0.25
	B	0.8 (1)	0.6 (2)	0.3 (2)	0.8 (2)	0.7 (3)	0.55 (14)
O1	x	0.7899 (8)	0.7904 (13)	0.7855 (11)	0.7918 (14)	0.7924 (17)	0.7896 (10)
	y	0.0905 (3)	0.0894 (7)	0.0883 (7)	0.0914 (9)	0.0934 (10)	0.0886 (6)
	z	0.25	0.25	0.25	0.25	0.25	0.25
	B	0.58 (6)	0.88 (12)	0.80 (10)	0.94 (14)	1.18 (15)	0.69 (9)
O2	x	0.2419 (7)	0.2421 (14)	0.2408 (11)	0.2425 (13)	0.2461 (17)	0.2454 (9)
	y	0.4330 (3)	0.4353 (7)	0.4346 (6)	0.4337 (8)	0.4321 (11)	0.4328 (6)
	z	0.25	0.25	0.25	0.25	0.25	0.25
	B	0.64 (6)	1.16 (13)	0.86 (11)	0.90 (16)	1.72 (18)	0.98 (10)
O3	x	0.2569 (4)	0.2524 (8)	0.2552 (8)	0.2545 (8)	0.2538 (9)	0.2534 (6)
	y	0.1628 (2)	0.1617 (6)	0.1622 (6)	0.1611 (8)	0.1629 (8)	0.1623 (5)
	z	0.0154 (3)	0.0162 (6)	0.0145 (6)	0.0138 (6)	0.0147 (7)	0.0154 (4)
	B	0.49 (4)	1.08 (11)	1.24 (9)	0.98 (13)	0.51 (11)	1.00 (3)

[a] Parenthesized figures represent *esd*'s
[b] $R=\Sigma[(F_o-F_c)^2/\Sigma wF_o^2]^{1/2}$ Weighted $R=[\Sigma w(|F_o|-|F_c|)^2/\Sigma wF_o^2]^{1/2}$
[c] Zachariasan [1967]

orientations (King and Finger 1979). The reflections selected for these measurements ranged from 25° to 40° 2θ. Intensities of all reflections in a hemisphere with $(\sin\theta)/\lambda \leqq 0.7$ were measured by an automated, four-circle diffractometer with graphite-monochromatized Mo$K\alpha$ radiation ($\lambda=0.7093$ Å). Omega step scans with 0.025° step increments and 4 second counting time per step were used. Digitized data were converted to graphical form and integrated peak intensities were determined by the method of Lehmann and Larsen (1974) with an option for manual intervention. Refinement conditions and refined structural parameters appear in Table 2, whereas refined anisotropic temperature parameters and the magnitudes and orientations of thermal vibration ellipsoids for chrysoberyl at room conditions are given in Table 3.

Data Collection at High Pressure

Flat, plate-like crystals approximately $100\times100\times40$ μm were mounted in a diamond-anvil pressure cell for x-ray diffraction, with an alcohol mixture of 4:1 methanol:ethanol as the hydrostatic pressure medium and 5 to 10 μm chips of ruby as an internal pressure calibrant. Pressure-cell design, loading, operation, and calibration were as described by Hazen and Finger (1982). Special care was taken to avoid x-ray shielding by the gasket portions of the diamond cell. A large gasket hole approximately 400 μm in diameter was employed, and the crystal was observed to remain centered in the hole throughout the experiments.

Unit-cell parameters of chrysoberyl were determined at five high pressures (Table 1). From 12 to 16 reflections were measured in eight equivalent positions by the method of Hamilton (1974), as modified by King and Finger (1979), in order to correct for errors in crystal centering and diffractometer alignment. The 2θ range of these reflections was 25° to 40° 2θ, the same as the room-pressure determination, in order to avoid any systematic errors in comparison of room-pressure and high-pressure data (Swanson et al. 1985). Each set of angular data was first refined without constraint, and the resultant "triclinic" cell was examined for conformity with the expected orthorhombic olivine symmetry. Unit-cell angles were 90° within two standard deviations (±0.04°) at all pressures studied. This result is evidence for hydrostaticity at all pressures as well as the absence of any distortional phase transition. Final lattice constants (Table 1) were obtained with the program of Ralph and Finger (1982) with the cell geometry constrained to be orthorhombic.

Table 3. Chrysoberyl anisotropic thermal parameters and magnitudes and orientations of vibration ellipsoids

Atom	Parameter	$\beta \times 10^4$	Axis	Displacement rms (Å)	Angle (°) with respect to:		
					a	*b*	*c*
Al1	β_{11}	70 (6)[a]	r_1	0.077 (6)	50 (17)	101 (23)	42 (22)
	β_{22}	16 (1)	r_2	0.084 (4)	64 (30)	135 (36)	124 (30)
	β_{33}	43 (4)	r_3	0.089 (5)	52 (20)	47 (33)	112 (27)
	β_{12}	2 (3)					
	β_{13}	6 (7)					
	β_{23}	0 (2)					
Al2[b]	β_{11}	47 (6)	r_1	0.067 (6)	54 (79)	144 (79)	90
	β_{22}	10 (1)	r_2	0.069 (4)	90	90	0
	β_{33}	31 (4)	r_3	0.069 (6)	36 (79)	54 (79)	90
	β_{12}	1 (3)					
Be[b]	β_{11}	99 (46)	r_1	0.09 (1)	90	90	0
	β_{22}	26 (5)	r_2	0.10 (2)	162 (67)	72 (67)	90
	β_{33}	55 (16)	r_3	0.11 (1)	72 (67)	18 (67)	90
	β_{12}	3 (10)					
O1[b]	β_{11}	93 (19)	r_1	0.069 (9)	94 (18)	4 (18)	90
	β_{22}	11 (3)	r_2	0.090 (10)	90	90	0
	β_{33}	53 (12)	r_3	0.096 (10)	4 (18)	86 (18)	90
	β_{12}	1 (7)					
O2[b]	β_{11}	92 (200)	r_1	0.077 (9)	62 (18)	28 (18)	90
	β_{22}	15 (26)	r_2	0.091 (10)	90	90	0
	β_{33}	55 (12)	r_3	0.100 (10)	28 (18)	118 (18)	90
	β_{12}	−8 (6)					
O3	β_{11}	56 (13)	r_1	0.062 (9)	51 (26)	100 (12)	41 (28)
	β_{22}	18 (2)	r_2	0.078 (8)	133 (25)	70 (17)	50 (28)
	β_{33}	32 (10)	r_3	0.093 (5)	68 (13)	23 (15)	96 (12)
	β_{12}	6 (4)					
	β_{13}	9 (7)					
	β_{23}	0 (3)					

[a] Parenthesized figures represent *esd*'s
[b] $\beta_{13}=\beta_{23}=0$. Atom is isotopic within *esd*'s

Intensity data for three-dimensional structure refinements were collected at 14, 31.5, 40, 54, and 62.5 (all ± 1) kbar. All accessible reflections with $(\sin\theta)/\lambda \leqq 0.7$ were measured. X-ray scattering intensities from chrysoberyl are extremely weak because the mineral contains only light atoms; intensities are further attenuated because of the small crystal encased in a pressure cell. Omega increments of 0.02° and counting times of 8 to 16 s per step were used to maximize the number and precision of observed reflections. The fixed-ϕ mode of data collection (Finger and King 1978) was used to optimize reflection accessibility and minimize attenuation by the diamond cell. Corrections were made for Lorentz and polarization effects, crystal absorption, and x-ray absorption by the diamond and beryllium components of the pressure cell (Hazen and Finger 1982). Conditions of high-pressure refinements as well as refined isotropic extinction coefficients (Zachariasen 1967), atomic positional parameters and isotropic thermal parameters are recorded in Table 2.

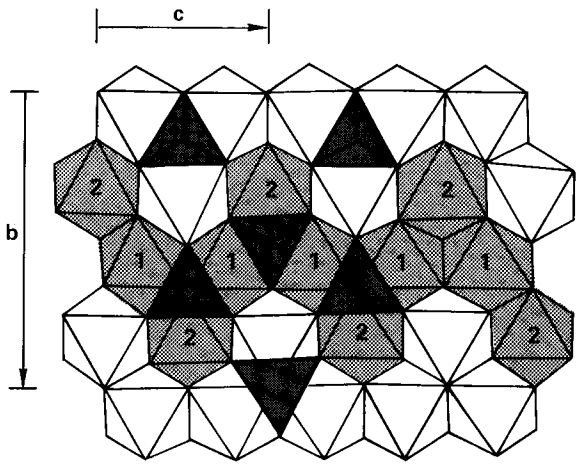

Fig. 1. The olivine-type structure in (100) projection (after Farrell et al. 1963). The structure may be visualized in terms of strips of M1 octahedral chains parallel to *c* with side-branching M2 octahedra. The unshaded octahedral strips are at $x=0$, whereas the shaded strip is at $x=0.5$. Tetrahedra cross-link the strips

Results

Room-pressure Refinement

The olivine-type structure consists of a hexagonal close-packed arrangement of oxygens in which one half of the octahedral sites and one eighth of the tetrahedral interstices are occupied (Fig. 1). There are two symmetrically distinct octahedral sites, designated M1 and M2, as well as one tetrahedral cation site. In silicate olivines the tetrahedral and octahedral cations are Si^{4+} and R^{2+}, whereas in chrysoberyl they are Be^{2+} and Al^{3+}, respectively. Bragg and

Table 4. Chrysoberyl selected distances (Å) and angles (°)

Bond/Angle		1 bar	14 kbar	31.5 kbar	40 kbar	54 kbar	62.5 kbar
Al1–O1	[2][a]	1.863 (2)[b]	1.853 (4)	1.855 (4)	1.853 (4)	1.856 (6)	1.840 (3)
Al1–O2	[2]	1.893 (2)	1.881 (4)	1.883 (4)	1.880 (4)	1.871 (6)	1.869 (3)
Al1–O3	[2]	1.911 (2)	1.888 (5)	1.894 (5)	1.882 (6)	1.890 (6)	1.882 (4)
Mean Al1–O		1.889	1.874	1.877	1.872	1.872	1.864
O1–Al1–O2	[2]	85.5 (1)	85.0 (2)	85.5 (2)	85.3 (2)	85.4 (3)	85.1 (3)
O1–Al1–O2	[2]	94.5 (1)	95.0 (2)	94.5 (2)	94.7 (2)	94.6 (3)	94.9 (2)
O1–Al1–O3	[2]	84.2 (1)	84.0 (2)	85.2 (2)	84.0 (2)	83.2 (3)	84.4 (2)
O1–Al1–O3	[2]	95.9 (1)	96.0 (2)	94.9 (2)	96.0 (2)	96.8 (3)	95.6 (2)
O2–Al1–O3	[2]	82.9 (1)	82.4 (2)	82.5 (2)	82.9 (3)	83.7 (3)	83.3 (2)
O2–Al1–O3	[2]	97.2 (1)	97.6 (2)	97.5 (2)	97.1 (3)	96.4 (3)	96.7 (2)
Al2–O1		1.940 (3)	1.948 (7)	1.964 (6)	1.923 (8)	1.889 (9)	1.942 (6)
Al2–O2		1.864 (3)	1.877 (7)	1.862 (6)	1.859 (7)	1.863 (10)	1.856 (5)
Al2–O3	[2]	1.894 (2)	1.906 (4)	1.889 (4)	1.891 (4)	1.887 (5)	1.887 (3)
Al2–O3	[2]	2.020 (2)	2.010 (4)	2.014 (4)	2.016 (5)	1.996 (5)	2.000 (3)
Mean Al2–O		1.939	1.942	1.939	1.933	1.920	1.929
O1–Al2–O3	[2]	79.3 (1)	78.5 (2)	79.2 (2)	78.7 (3)	79.5 (3)	78.8 (2)
O1–Al2–O3	[2]	91.4 (1)	91.5 (2)	91.1 (2)	91.6 (3)	91.3 (3)	91.4 (2)
O2–Al2–O3	[2]	93.9 (1)	93.9 (2)	93.8 (2)	93.7 (3)	94.0 (3)	94.3 (2)
O2–Al2–O3	[2]	94.3 (1)	95.2 (2)	95.0 (2)	95.1 (2)	94.3 (3)	94.4 (2)
O3–Al2–O3	[2]	89.7 (1)	90.0 (1)	89.8 (1)	90.1 (2)	89.8 (2)	89.9 (1)
O3–Al2–O3		79.1 (1)	79.0 (3)	79.3 (2)	79.4 (3)	79.8 (3)	79.2 (2)
O3–Al2–O3		100.3 (1)	99.6 (3)	99.7 (2)	99.0 (3)	99.5 (3)	99.7 (3)
Be–O1		1.581 (7)	1.596 (11)	1.574 (9)	1.591 (11)	1.581 (13)	1.566 (8)
Be–O2		1.694 (6)	1.630 (15)	1.668 (13)	1.654 (17)	1.669 (20)	1.665 (11)
Be–O3	[2]	1.641 (4)	1.649 (8)	1.630 (6)	1.644 (9)	1.653 (10)	1.644 (7)
Mean Be–O		1.639	1.631	1.625	1.633	1.639	1.630
O1–Be–O2		116.3 (4)	117.9 (8)	114.9 (6)	117.5 (9)	119.5 (10)	119.0 (4)
O1–Be–O3	[2]	118.7 (2)	118.3 (5)	118.9 (4)	118.0 (6)	117.9 (6)	117.6 (6)
O2–Be–O3	[2]	98.0 (3)	98.5 (6)	98.1 (4)	98.0 (6)	98.0 (6)	97.7 (4)
O3–Be–O3		103.2 (3)	101.7 (7)	104.2 (6)	103.1 (8)	101.5 (8)	101.7 (5)
O1–Be		1.581 (7)	1.596 (11)	1.574 (9)	1.591 (11)	1.581 (13)	1.566 (8)
O1–Al1	[2]	1.863 (2)	1.881 (4)	1.855 (4)	1.853 (4)	1.856 (6)	1.840 (3)
O1–Al2		1.940 (3)	1.948 (7)	1.964 (6)	1.923 (8)	1.889 (9)	1.942 (6)
Be–O1–Al1	[2]	120.4 (2)	119.9 (4)	121.6 (3)	119.5 (4)	118.8 (5)	120.5 (3)
Be–O1–Al2		117.0 (3)	117.7 (6)	116.3 (5)	118.2 (7)	119.3 (8)	117.0 (5)
Al1–O1–Al1		94.7 (1)	95.1 (3)	94.7 (3)	94.7 (3)	94.2 (4)	95.2 (2)
Al1–O1–Al2	[2]	99.9 (1)	99.9 (2)	98.8 (2)	100.2 (3)	100.6 (3)	99.6 (2)
O2–Be		1.694 (6)	1.630 (15)	1.668 (13)	1.654 (17)	1.669 (20)	1.665 (11)
O2–Al1	[2]	1.893 (2)	1.881 (4)	1.883 (4)	1.880 (4)	1.871 (6)	1.869 (3)
O2–Al2		1.864 (3)	1.877 (7)	1.862 (6)	1.859 (7)	1.863 (10)	1.856 (5)
Be–O2–Al1	[2]	88.8 (2)	89.8 (4)	89.0 (3)	89.2 (4)	89.1 (5)	89.3 (3)
Be–O2–Al2		116.8 (3)	116.5 (5)	117.6 (4)	116.6 (5)	115.3 (6)	115.3 (4)
Al1–O2–Al1		92.8 (1)	93.3 (3)	92.9 (2)	93.0 (3)	93.3 (4)	93.3 (2)
Al1–O2–Al2	[2]	128.7 (1)	128.1 (2)	128.2 (2)	128.5 (2)	128.9 (3)	128.8 (2)
O3–Be		1.641 (4)	1.649 (8)	1.630 (6)	1.644 (9)	1.653 (10)	1.644 (7)
O3–Al1		1.911 (2)	1.888 (5)	1.894 (5)	1.882 (6)	1.890 (6)	1.882 (4)
O3–Al2		1.894 (2)	1.906 (4)	1.889 (4)	1.891 (4)	1.887 (5)	1.887 (3)
O3–Al2		2.020 (2)	2.010 (4)	2.014 (5)	2.016 (5)	1.996 (5)	2.000 (3)
Be–O3–Al1		89.8 (1)	89.0 (5)	89.8 (4)	89.4 (6)	88.9 (6)	89.4 (4)
Be–O3–Al2		88.9 (2)	89.6 (4)	88.2 (3)	88.7 (4)	89.3 (4)	89.5 (3)
Be–O3–Al2		117.8 (2)	117.4 (4)	117.8 (3)	117.5 (4)	117.2 (5)	117.0 (3)
Al1–O3–Al2		95.5 (1)	96.5 (2)	95.8 (2)	96.0 (2)	95.7 (2)	96.1 (1)
Al1–O3–Al2		123.6 (1)	123.6 (2)	123.9 (2)	124.5 (2)	124.0 (3)	123.7 (2)
Al2–O3–Al2		130.1 (1)	129.6 (3)	129.9 (3)	129.3 (4)	130.2 (4)	129.9 (3)

[a] Bracketed figures represent bond or angle multiplicities
[b] Parenthesized figures represent *esd*'s

Table 5. Chrysoberyl polyhedral volume and distortion

Atom/Parameter		1 bar	14 kbar	31.5 kbar	40 kbar	54 kbar	62.5 kbar
Al1	Vol (Å^3)	8.84 (1)[a]	8.63 (2)	8.69 (2)	8.60 (3)	8.62 (4)	8.50 (2)
	QE[b]	1.010 (1)	1.012 (1)	1.010 (1)	1.011 (1)	1.011 (1)	1.010 (1)
	AV[c]	38	43	36	39	39	36
Al2	Vol(Å^3)	9.52 (1)	9.57 (3)	9.52 (3)	9.43 (3)	9.26 (4)	9.37 (3)
	QE	1.014 (2)	1.015 (4)	1.014 (3)	1.015 (4)	1.013 (5)	1.015 (3)
	AV	48	52	48	48	44	49
Be	Vol (Å^3)	2.19 (1)	2.15 (2)	2.13 (2)	2.16 (2)	2.18 (2)	2.14 (1)
	QE	1.023	1.023	1.022	1.023	1.024	1.025
	AV	104	105	98	104	113	117

[a] Parenthesized figures represent *esd*'s

[b] Quadratic elongation $\langle\lambda\rangle = \sum_{i=1}^{n} [(l_i/l_o)^2/n]$, where l_o is the center-to-vertex distance of a regular polyhedron of the same volume, n is the coordination number, and l_i is an observed cation-anion distance

[c] Angle Variance $\sigma^2 = \sum_{i=1}^{n} [(\theta_i - \theta_o)^2/n]$, where θ_o is the ideal bond angle for a regular polyhedron, n is the coordination number, and θ_i is an anion-cation-anion angle

Brown (1926) first determined the chrysoberyl structure, which is orthorhombic with space group *Pbmn* (in the non-standard setting of silicate olivine; $b > c > a$) and $Z = 4$. Subsequent refinements by Farrell et al. (1963) and J.W. Downs (unpublished data 1985) have confirmed the earlier determination.

The present room-pressure structure refinement is in agreement with previous studies. Selected bond distances and angles are listed in Table 4, and cation polyhedral volumes and distortion indices appear in Table 5. The beryllium tetrahedron (point symmetry *m*) is moderately distorted, with three adjacent shared oxygen-oxygen edges of approximately 2.5 Å, and three unshared edges of approximately 2.8 Å. The O – Be – O angles of this tetrahedron range from 98° to 119° compared to the ideal value of 109.5°; the shortest O – Be – O angles correspond to shared O – O edges. The Be – O distances display a range from 1.58 to 1.69 Å.

The Al1 octahedron (point symmetry $\bar{1}$) is close to regular, with Al – O bond distance ranging from 1.86 to 1.91 Å and O – Al – O angle deviating by 7° or less from the ideal 90° value. The Al2 octahedron (point symmetry *m*) is somewhat more distorted with cation-anion distances from 1.86 to 2.02 Å and angles from 79° to 100°. Oxygen-oxygen distances in the two aluminium octahedra that share polyhedral edges are shorter than unshared O – O distances.

The three symmetrically distinct oxygen anions are all four coordinated to one tetrahedral and three octahedral cations, in a distorted tetrahedral arrangement. Cation-anion-cation angles deviate by as much as 20° from the ideal tetrahedral 109.5° value.

Thermal vibration ellipsoids of cations in chrysoberyl (Table 3) are nearly isotropic, thus reflecting the near regular coordination of these atoms. The three oxygen anions display more anisotropic vibration ellipsoids, with minimum vibration amplitudes approximately along the direction of the short Be – O bonds.

Axial Compressibilities and Bulk Moduli

Axial compressibilities and equation-of-state parameters for chrysoberyl have been calculated from unit-cell parameters at several pressures (Table 1 and Fig. 2). Pressure-variation of the three unit-cell edges were described with the expression:

$$a = a_0 - d_1 P + d_2 P^2,$$

where a_0 is the value of the cell parameter at room pressure, and d_1 and d_2 are fitted parameters. The d_2 parameters

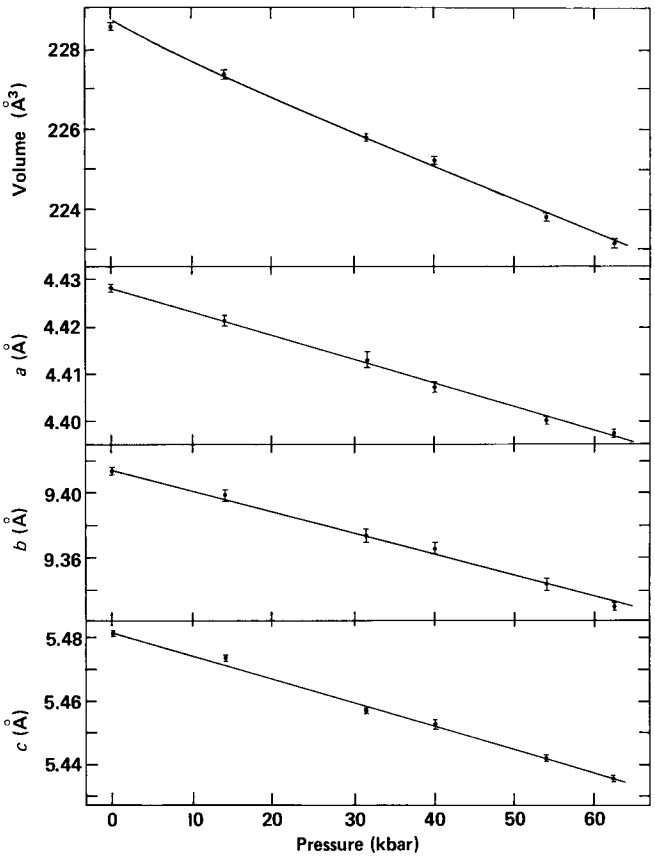

Fig. 2. Unit-cell dimensions and volume are plotted versus pressure

for a and c axes are positive, whereas that for the b axis is negative; the magnitudes of these coefficients are less than two estimated standard deviations, however, so no significant curvature can be ascribed to axial compression. The resultant expressions for average axial compression between room pressure and 62.5 kbar are:

$a = 4.4278 \pm 0.0007 - 0.000497 \pm 0.000017 P$
$(\beta_a = 1.12 \pm 0.04 \times 10^{-4}\ \text{kbar}^{-1})$
$b = 9.4177 \pm 0.0014 - 0.00138 \pm 0.00005 P$
$(\beta_b = 1.46 \pm 0.05 \times 10^{-4}\ \text{kbar}^{-1})$
$c = 5.4808 \pm 0.0008 - 0.000716 \pm 0.000018 P$
$(\beta_c = 1.31 \pm 0.03 \times 10^{-4}\ \text{kbar}^{-1})$

Note that a, b, and c are unit-cell edge lengths in Å, whereas β's with subscripts represent axial compressibilities (Hazen and Finger 1982). Calculated axial compression ratios are thus $\beta_a : \beta_b : \beta_c = 1.00 : 1.30 : 1.17$, which agree within error with the values 1.00:1.20:1.13 observed by Wang et al. (1975).

The bulk modulus, K, of chrysoberyl was calculated by least-squares fit of pressure-volume data to a Birch-Murnaghan equation-of-state:

$$P = \tfrac{3}{2} K_0 \left[\left(\frac{V_0}{V}\right)^{7/3} - \left(\frac{V_0}{V}\right)^{5/3} \right] \left\{ 1 - \tfrac{3}{4}(4 - K_0') \left[\left(\frac{V_0}{V}\right)^{2/3} - 1 \right] \right\}.$$

If the pressure derivative of the bulk modulus, K', is assumed to be 4, then $K = 2.42 \pm 0.05$ Mbar, in close agreement with the 2.40 Mbar value of Wang et al. (1975). Alternatively, if the 2.40 Mbar bulk modulus of Wang et al. is assumed, then the calculated value of K' from the present pressure-volume data is 3.9 ± 1.6.

Crystal Structures at High Pressure

Examination of bond distances and angles of chrysoberyl as a function of pressure (Table 4) reveals that the principal changes in structure are shortening of interatomic distances. Bond angles both in cation and anion coordination polyhedra do not appear to vary significantly, but cation-anion distances shorten significantly (Table 4). "Polyhedral bulk modulus," K_p, is a particularly revealing parameter in describing silicate compression. It is defined as:

$$K_p = -V_p \, \partial P / \partial V_p,$$

where V_p is the polyhedral volume, defined by the positions of coordinating oxygens, and P is the hydrostatic pressure. Note that the local stress environment of a given polyhedron may not be equal to the external hydrostatic pressure; polyhedral bulk modulus, therefore, is not strictly analogous to crystal bulk modulus. The largest changes occur in the A11 octahedron, which has an average bond compressibility of approximately $1.8 \times 10^{-4}\ \text{kbar}^{-1}$, and a corresponding polyhedral bulk modulus[1] of 1.8 ± 0.4 Mbar. The A12 octahedron and the Be tetrahedron are both less compressible than A11, with average A12–O and Be–O bond compressibilities of $1.1 \times 10^{-4}\ \text{kbar}^{-1}$ and corresponding polyhedral bulk moduli of approximately 3 ± 1 Mbar.

Discussion

Comparison with Silicate Olivines at High Pressure

Why do silicate olivines compress anisotropically, while chrysoberyl compresses more nearly isotropically? An important difference between high-pressure structures of the two minerals is the *relative* compressibility of octahedral versus tetrahedral cation-oxygen bonds. In silicate olivines the octahedral M1–O bonds are *several times* more compressible than tetrahedral Si–O bonds. Rigid silicon tetrahedra restrict compression of olivine parallel to the a axis because tetrahedra alternate with M1 octahedra in a layer-like pattern (Fig. 3a). Compression of olivine parallel to a is thus approximately the average of M1–O and Si–O bond compressibilities. The compressibility parallel to b, on the other hand, is nearly equal to that of the relatively compressible M1–O bonds; the staggered distribution of tetrahedra in the (100) plane (Fig. 1) does not restrict compression significantly. Thus the axial compression ratio, β_a/β_b, may be approximated by the simple expression:

$$\beta_a/\beta_b \approx (\beta_{M1} + \beta_T)/2\beta_{M1}.$$

In forsterite, with $\beta_{Mg1} = 3.5 \times 10^{-4}\ \text{kbar}^{-1}$ and $\beta_{Si} \approx 0.6 \times 10^{-4}\ \text{kbar}^{-1}$ (Hazen and Finger 1980), the estimated compression anisotropy is:

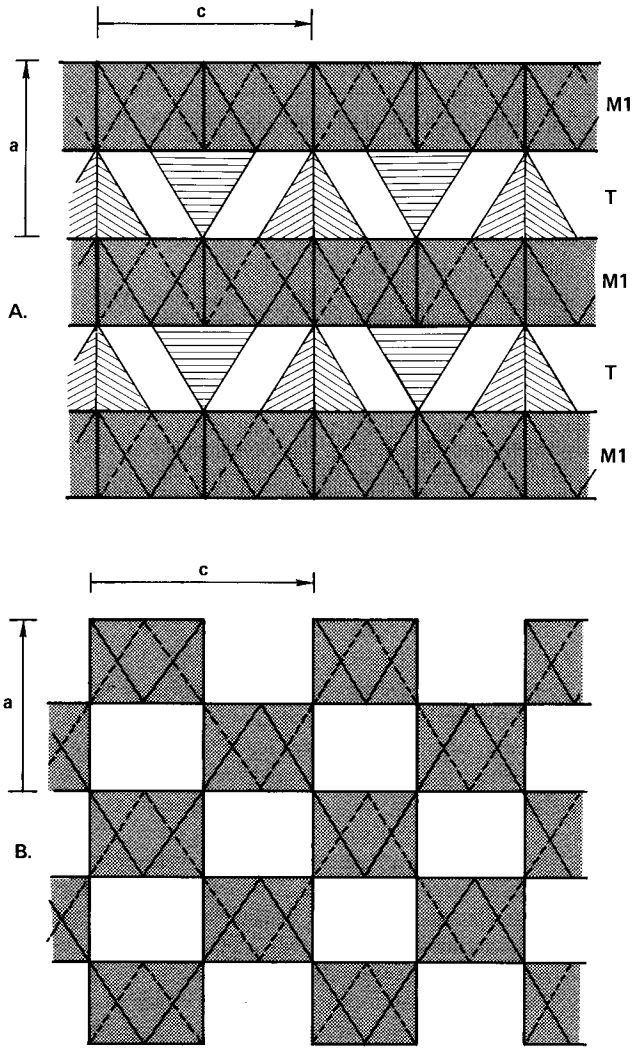

Fig. 3A, B. The olivine-type structure in (010) projections. **(A)** Cation polyhedra near $y = 0$ (and $y = 0.50$) include strips of M1 octahedra parallel to c, cross-linked by tetrahedra with cations at $y = \pm 0.09$ (and $y = 0.50 \pm 0.09$). The M1 octahedra are the most compressible polyhedra in chrysoberyl and in forsterite. **(B).** Cation polyhedra near $y = \pm 0.25$; the M2 octahedra form a checkerboard pattern

$\beta_a/\beta_b \approx (3.5+0.6)/2(3.5) = 0.59,$

which compares reasonably well with the observed value of 0.50.

Chrysoberyl, in contrast to silicate olivines, is nearly isotropic because M1 – O and T – O bond compressibilities are similar. Octahedral Al1 – O bonds in chrysoberyl compress approximately 1.8×10^{-4} kbar^{-1}, whereas tetrahedral Be – O bonds compress about 1.1×10^{-4} kbar^{-1}. The estimated anisotropy is thus:

$\beta_a/\beta_b \approx (1.8+1.1)/2(1.8) = 0.81,$

compared to the observed value of 0.77.

Two factors thus contribute to the anisotropy of olivine-type compounds. The structure, itself, is inherently anisotropic, because of the distribution of cation coordination octahedra and tetrahedra (Figs. 1 and 3). However, structural anisotropy is only a necessary condition – not a sufficient one – for compression anisotropy. The octahedral and tetrahedral units must also have significantly different cation-oxygen compressibilities in order for the inherent structural anisotropy (i.e., the planar distribution of polyhedra illustrated in Figures 1 and 3) to be manifest in crystal properties.

The magnitude of olivine anisotropy thus appears to be a function of the difference in compressibility between the octahedral and tetrahedral cation polyhedra. In forsterite the M1 magnesium octahedron is almost an order of magnitude more compressible than the silicon tetrahedron; the resulting elastic anisotropy is large. In chrysoberyl, on the other hand, the average compressibility of Al – O and Be – O bonds are more nearly equal, so the compression is much less anisotropic.

Anomalies in Velocity-Density Systematics

More than a decade ago chrysoberyl was recognized as an "anomaly in velocity-density systematics" (Wang et al. 1975). Chrysoberyl did not fit "normal" velocity-density plots that display increasing bulk sound velocity with density for isomorphous mineral series (see e.g., Liebermann 1982). An important conclusion of high-pressure crystal structure determinations, including the present study of chrysoberyl, is that cation valence, independent of atomic number, can be a key factor in mineral bulk modulus: Polyhedral bulk modulus is proportional to cation formal charge (Hazen and Finger 1979). Isomorphous minerals that are related by mixed-valence substitutions, therefore, are not expected to conform to simple velocity-density systematics. The bulk modulus of chrysoberyl, for example, is controlled primarily by trivalent aluminum octahedral compression and is thus significantly greater than the bulk moduli of silicate olivines, which have divalent cations in octahedral coordination.

Another striking example of the effects of mixed-valence substitution is provided by the scheelite-type compounds, which have equal numbers of 8-coordinated A cations and tetrahedrally-coordinated B cations in an ABO_4 structure (Hazen et al. 1985). Observed valence combinations range from $NaIO_4$ (+1 and +7) to $ZrGeO_4$ (+4 and +4), with many common examples of 2–6 and 3–5 valence combinations as well. The bulk moduli of these compounds are governed by the compressibilities of the large, 8-coordinated A sites. The bulk modulus of zirconium germanate, for example, is several times that of sodium tungstate because of the great differences in compressibility of Na^+ and Zr^{4+} coordination polyhedra. Any attempt to derive a velocity-density relationship for all scheelite-type compounds, without including a factor for A cation valence, will fail.

In addition to olivine, several important rock-forming mantle silicates display mixed-valence substitution; these minerals are also expected to have "anomalous" velocity-density systematics. Mantle pyroxenes ($R^{2+}SiO_3$) are often aluminous, thus implying substitutions of the form $2Al^{3+} \rightleftharpoons R^{2+} + Si^{4+}$ or $Al^{3+} + Na^+ \rightleftharpoons 2R^{2+}$. Mantle garnets, with idealized formula $A_3^{VIII}B_2^{IV}C_3^{IV}O_{12}$, are subject to complex mixed valence substitutions. The large A site, though usually occupied by divalent Ca, Mg or Fe, may incorporate either monovalent alkalis or trivalent rare earth elements. The octahedrally coordinated B site is occupied by trivalent Al or Fe in most crustal garnets, but in high-pressure forms both Si^{4+} and divalent cations may be incorporated. It is possible, therefore, to accommodate pyroxene stoichiometry in a garnet of the form $R_3^{VIII}(RSi)^{VI}Si_3^{IV}O_{12}$, where R represents divalent cations. Perovskite-type ABO_3 compounds, which are receiving considerable attention as the probable dominant mineral species of the earth's lower mantle, are subject to the same types of mixed-valence substitutions that are observed in olivines, pyroxenes and garnets. The magnesium silicate perovskite ($Mg^nSi^{VI}O_3$; $n>8$), for example, could have substitutions of +1, +2 and +3 cations in the large n-coordinated site and +3, +4, and +5 cations in the octahedral site. Given the significant effects of mixed-valence substitution on mineral compression, great care must be taken when applying velocity-density systematics to these chemically complex phases.

Acknowledgments. The author thanks A.Y. Au, L.W. Finger, and J.W. Downs for stimulating discussions, and F.R. Boyd, B.O. Mysen, and H.S. Yoder, Jr. and four anonymous referees for their constructive reviews of the manuscript. This work was supported in part by National Science Foundation Grant EAR83-19209 and EAR84-19982.

References

Au AY, Hazen RM (1985) Polyhedral modeling of the elastic properties of corundum ($\alpha - Al_2O_3$) and chrysoberyl (Al_2BeO_4). Geophys Res Lett 12:725–728

Barton MD (1986) Phase equilibria and thermodynamic properties of minerals in the $BeO - Al_2O_3 - SiO_2 - H_2O$ (BASH) system, with petrologic applications. Am Mineral 71:277–300

Bragg WL, Brown GB (1926) Die Struktur des Olivins. Z Kristallogr 63:538

Farrell EF, Fang JH, Newnham RE (1963) Refinement of the chrysoberyl structure. Am Mineral 48:804–810

Finger LW, King HE (1978) A revised method of operation of the single-crystal diamond cell and refinement of the structure of NaCl at 32 kbar. Am Mineral 63:337–342

Graham EK, Barsch GR (1969) Elastic constants of single-crystal forsterite as a function of temperature and pressure. J Geophys Res 74:5949–5960

Hamilton WC (1974) Angle settings for four-circle diffractometers. In: International Tables for X-ray Crystallography, 4:273–284. Kynoch Press, Birmingham, England

Hazen RM (1977) Effects of temperature and pressure on the crystal structure of ferromagnesian olivine. Am Mineral 62:309–315

Hazen RM, Finger LW (1979) Bulk-modulus-volume relationship for cation-anion polyhedra, J Geophys Res 84:6723–6728

Hazen RM, Finger LW (1980) Crystal structure of forsterite at 40 kbar. Carnegie Inst Washington Yearbook 79:364–367

Hazen RM, Finger LW (1982) Comparative crystal chemistry. Wiley, New York

Hazen RM, Finger LW, Mariathasan JWE (1985) High-pressure crystal chemistry of scheelite-type tungstates and molybdates. J Phys Chem Solids 46:253–263

King HE, Finger LW (1979) Diffracted beam crystal centering and its application to high-pressure crystallography. J Appl Crystallogr 12:374–378

Kudoh Y, Takeuchi Y (1985) The crystal structure of forsterite Mg_2SiO_4 under high pressures up to 149 kbar. Z Kristallogr 171:291–302

Kudoh Y, Takeda H (1986) Single crystal x-ray diffraction study on bond compressibility of fayalite, Fe_2SiO_4 and rutile, TiO_2 under high pressure. Proc 10th AIRAPT Conf, in press

Kumazawa M, Anderson OL (1969) Elastic moduli, pressure derivatives, and temperature derivatives of single-crystal olivine and single-crystal forsterite. J Geophys Res 74:5961–5972

Lehmann MS, Larsen FK (1974) A method for location of the peaks in step-scan-measured Bragg reflections. Acta Crystallogr A30:580–584

Liebermann RC (1982) Elasticity of minerals at high temperature and pressure. In: Schreyer W (ed.) High-Pressure Research in Geoscience. E. Schweizerbart'sche Verlagsbuchhandlung, Stuttgart

Ralph RL, Finger LW (1982) A computer program for refinement of crystal orientation matrix and lattice constants from diffractometer data with lattice symmetry constants. J Appl Crystallogr 15:537–539

Sharp ZD, Hazen RM, Finger LW (1986) Structural refinements of monticellite to 60 kbar. GSA Abstracts with Program, in press

Shimizu H, Bassett WA, Brody EM (1982) Brillouin-scattering measurements of single-crystal forsterite to 40 kbar at room temperature. J Appl Phys 53:620–626

Sumino Y, Nishizawa O, Goto T, Ohno I, Ozima M (1977) Temperature variation of elastic constants of single-crystal forsterite between −190° and 400° C. J Phys Earth 25:377–392

Suzuki I, Anderson OL, Sumino Y (1983) Elastic properties of a single-crystal forsterite Mg_2SiO_4, up to 1,200 K. Phys Chem Minerals 10:38–46

Swanson DK, Weidner DJ, Prewitt CT, Kandelin JJ (1985) Single-crystal compression of $\gamma-Mg_2SiO_4$ (abstract). Trans Am Geophys Union (EOS) 66:370

Wang H, Gupta MC, Simmons G (1975) Chrysoberyl (Al_2BeO_4): Anomaly in velocity-density systematics. J Geophys Res 80:3761–3764

Zachariasen WH (1967) A general theory of x-ray diffraction in crystals. Acta Crystallogr 23:558–564

Received April 1, 1986